

and Lobell, 2007). There is clear evidence that irrigation leads to local cooling of several degrees (Kueppers et al., 2007). Irrigation also affects cloudiness and precipitation (Puma and Cook, 2010). In the United States, DeAngelis et al. (2010) found that irrigation in the Great Plains in the summer produced enhanced precipitation in the Midwest 1000 km to the northeast.

#### 8.3.5.6 Conclusions

There is still a rather wide range of estimates of the albedo change due to anthropogenic land use change, and its RF. Although most published studies provide an estimate close to  $-0.2 \text{ W m}^{-2}$ , there is convincing evidence that it may be somewhat weaker as the albedo difference between natural and anthropogenic land cover may have been overestimated. In addition, non-radiative impact of land use have a similar magnitude, and may be of opposite sign, as the albedo effect (though these are not part of RF). A comparison of the impact of land use change according to seven climate models showed a wide range of results (Pitman et al., 2009), partly due to difference in the implementation of land cover change, but mostly due to different assumptions on ecosystem albedo, plant phenology and evapotranspiration. There is no agreement on the sign of the temperature change induced by anthropogenic land use change. It is very likely that land use change led to an increase of the Earth albedo with a RF of  $-0.15 \pm 0.10 \text{ W m}^{-2}$ , but a net cooling of the surface accounting for processes that are not limited to the albedo is about as likely as not.

## 8.4 Natural Radiative Forcing Changes: Solar and Volcanic

Several natural drivers of climate change operate on multiple time scales. Solar variability takes place at many time scales that include centennial and millennial scales (Helama et al., 2010), as the radiant energy output of the Sun changes. Also, variations in the astronomical alignment of the Sun and the Earth (Milankovitch cycles) induce cyclical changes in RF, but this is substantial only at millennial and longer time scales (see Section 5.2.1.1). Volcanic forcing is highly episodic, but can have dramatic, rapid impacts on climate. No major asteroid impacts occurred during the reference period (1750–2012) and thus this effect is not considered here. This section discusses solar and volcanic forcings, the two dominant natural contributors of climate change since the pre-industrial time.

### 8.4.1 Solar Irradiance

In earlier IPCC reports the forcing was estimated as the instantaneous RF at TOA. However, due to wavelength-albedo dependence, solar radiation-wavelength dependence and absorption within the stratosphere and the resulting stratospheric adjustment, the RF is reduced to about 78% of the TOA instantaneous RF (Gray et al., 2009). There is *low confidence* in the exact value of this number, which can be model and time scale dependent (Gregory et al., 2004; Hansen et al., 2005). AR4 gives an 11-year running mean instantaneous TOA RF between 1750 and the present of  $0.12 \text{ W m}^{-2}$  with a range of estimates of 0.06 to  $0.30 \text{ W m}^{-2}$ , equivalent to a RF of  $0.09 \text{ W m}^{-2}$  with a range of 0.05 to  $0.23 \text{ W m}^{-2}$ . For a consistent treatment of all forcing agents, hereafter we use

RF while numbers quoted from AR4 will be provided both as RF and instantaneous RF at TOA.

#### 8.4.1.1 Satellite Measurements of Total Solar Irradiance

Total solar irradiance (TSI) measured by the Total Irradiance Monitor (TIM) on the spaceborne Solar Radiation and Climate Experiment (SORCE) is  $1360.8 \pm 0.5 \text{ W m}^{-2}$  during 2008 (Kopp and Lean, 2011) which is  $\sim 4.5 \text{ W m}^{-2}$  lower than the Physikalisch-Meteorologisches Observatorium Davos (PMOD) TSI composite during 2008 (Frohlich, 2009). The difference is probably due to instrumental biases in measurements prior to TIM. Measurements with the PREcision MONitor Sensor (PREMOS) instrument support the TIM absolute values (Kopp and Lean, 2011). The TIM calibration is also better linked to national standards which provides further support that it is the most accurate (see Supplementary Material Section 8.SM.6). Given the lower TIM TSI values relative to currently used standards, most general circulation models are calibrated to incorrectly high values. However, the few tenths of a percent bias in the absolute TSI value has minimal consequences for climate simulations because the larger uncertainties in cloud properties have a greater effect on the radiative balance. As the maximum-to-minimum TSI relative change is well-constrained from observations, and historical variations are calculated as changes relative to modern values, a revision of the absolute value of TSI affects RF by the same fraction as it affects TSI. The downward revision of TIM TSI with respect to PMOD, being 0.3%, thus has a negligible impact on RF, which is given with a relative uncertainty of several tenths of a percent.

Since 1978, several independent space-based instruments have directly measured the TSI. Three main composite series were constructed, referred to as the Active Cavity Radiometer Irradiance Monitor (ACRIM) (Willson and Mordvinov, 2003), the Royal Meteorological Institute of Belgium (RMIB) (Dewitte et al., 2004) and the PMOD (Frohlich, 2006) series. There are two major differences between ACRIM and PMOD. The first is the rapid drift in calibration between PMOD and ACRIM before 1981. This arises because both composites employ the Hickey–Frieden (HF) radiometer data for this interval, while a re-evaluation of the early HF degradation has been implemented by PMOD but not by ACRIM. The second one, involving also RMIB, is the bridging of the gap between the end of ACRIM I (mid-1989) and the beginning of ACRIM II (late 1991) observations, as it is possible that a change in HF data occurred during this gap. This possibility is neglected in ACRIM and thus its TSI increases by more than  $0.5 \text{ W m}^{-2}$  during solar cycle (SC) 22. These differences lead to different long-term TSI trends in the three composites (see Figure 8.10): ACRIM rises until 1996 and subsequently declines, RMIB has an upward trend through 2008 and PMOD shows a decline since 1986 which unlike the other two composites, follows the solar-cycle-averaged sunspot number (Lockwood, 2010). Moreover, the ACRIM trend implies that the TSI on time scales longer than the SC is positively correlated with the cosmic ray variation indicating a decline in TSI throughout most of the 20th century (the opposite to most TSI reconstructions produced to date; see Section 8.4.1.2). Furthermore, extrapolating the ACRIM TSI long-term drift would imply a brighter Sun in the Maunder minimum (MM) than now, again opposite to most TSI reconstructions (Lockwood and Frohlich, 2008). Finally, analysis of instrument degradation and pointing issues (Lee et al., 1995) and independent modeling based on solar magnetograms (Wenzler et al.,

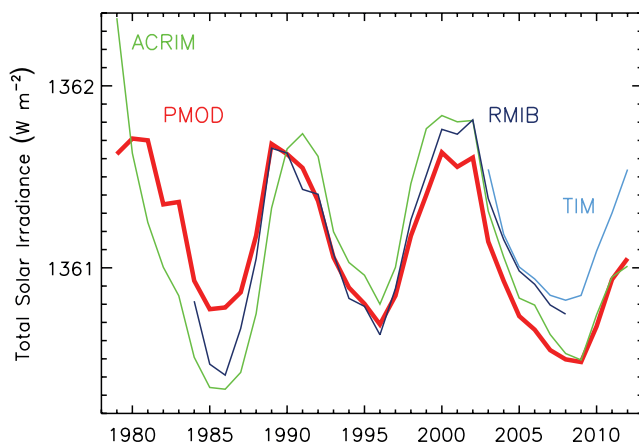


**Figure 8.10** | Annual average composites of measured total solar irradiance: The Active Cavity Radiometer Irradiance Monitor (ACRIM) (Willson and Mordvinov, 2003), the Physikalisch-Meteorologisches Observatorium Davos (PMOD) (Frohlich, 2006) and the Royal Meteorological Institute of Belgium (RMIB) (Dewitte et al., 2004). These composites are standardized to the annual average (2003–2012) Total Irradiance Monitor (TIM) (Kopp and Lean, 2011) measurements that are also shown.

2009; Ball et al., 2012), confirm the need for correction of HF data, and we conclude that PMOD is more accurate than the other composites.

TSI variations of approximately 0.1% were observed between the maximum and minimum of the 11-year SC in the three composites mentioned above (Kopp and Lean, 2011). This variation is mainly due to an interplay between relatively dark sunspots, bright faculae and bright network elements (Foukal and Lean, 1988; see Section 5.2.1.2). A declining trend since 1986 in PMOD solar minima is evidenced in Figure 8.10. Considering the PMOD solar minima values of 1986 and 2008, the RF is  $-0.04 \text{ W m}^{-2}$ . Our assessment of the uncertainty range of changes in TSI between 1986 and 2008 is  $-0.08$  to  $0.0 \text{ W m}^{-2}$  and thus very likely negative, and includes the uncertainty in the PMOD data (Frohlich, 2009; see Supplementary Material Section 8.SM.6) but is extended to also take into account the uncertainty of combining the satellite data.

For incorporation of TIM data with the previous and overlapping data, in Figure 8.10 we have standardized the composite time series to the TIM series (over 2003–2012, the procedure is explained in Supplementary Material Section 8.SM.6. Moreover as we consider annual averages, ACRIM and PMOD start at 1979 because for 1978 both composites have only two months of data.

#### 8.4.1.2 Total Solar Irradiance Variations Since Preindustrial Time

The year 1750, which is used as the preindustrial reference for estimating RF, corresponds to a maximum of the 11-year SC. Trend analysis is usually performed over the minima of the solar cycles that are more stable. For such trend estimates, it is then better to use the closest SC minimum, which is in 1745. To avoid trends caused by comparing different portions of the solar cycle, we analyze TSI changes using multi-year running means. For the best estimate we use a recent TSI reconstruction by Krivova et al. (2010) between 1745 and 1973 and from 1974 to 2012 by Ball et al. (2012). The reconstruction is based

on physical modeling of the evolution of solar surface magnetic flux, and its relationship with sunspot group number (before 1974) and sunspot umbra and penumbra and faculae afterwards. This provides a more detailed reconstruction than other models (see the time series in Supplementary Material Table 8.SM.3). The best estimate from our assessment of the most reliable TSI reconstruction gives a 7-year running mean RF between the minima of 1745 and 2008 of  $0.05 \text{ W m}^{-2}$ . Our assessment of the range of RF from TSI changes is  $0.0$  to  $0.10 \text{ W m}^{-2}$  which covers several updated reconstructions using the same 7-year running mean past-to-present minima years (Wang et al., 2005; Steinhilber et al., 2009; Delaygue and Bard, 2011), see Supplementary Material Table 8.SM.4. All reconstructions rely on indirect proxies that inherently do not give consistent results. There are relatively large discrepancies among the models (see Figure 8.11). With these considerations, we adopt this value and range for AR5. This RF is almost half of that in AR4, in part because the AR4 estimate was based on the previous solar cycle minimum while the AR5 estimate includes the drop of TSI in 2008 compared to the previous two SC minima (see 8.4.1). Concerning the uncertainty range, in AR4 the upper limit corresponded to the reconstruction of Lean (2000), based on the reduced brightness of non-cycling Sun-like stars assumed typical of a Maunder minimum (MM) state. The use of such stellar analogues was based on the work of Baliunas and Jastrow (1990), but more recent surveys have not reproduced their results and suggest that the selection of the original set was flawed (Hall and Lockwood, 2004; Wright, 2004); the lower limit from 1750 to present in AR4 was due to the assumed increase in the amplitude of the 11-year cycle only. Thus the RF and uncertainty range have been obtained in a different way in AR5 compared to AR4. Maxima to maxima RF give a higher estimate than minima to minima RF, but the latter is more relevant for changes in solar activity. Given the *medium agreement* and *medium evidence*, this RF value has a *medium confidence level* (although confidence is higher for the last three decades). Figure 8.11 shows several TSI reconstructions modelled using sunspot group numbers (Wang et al., 2005; Krivova et al., 2010;

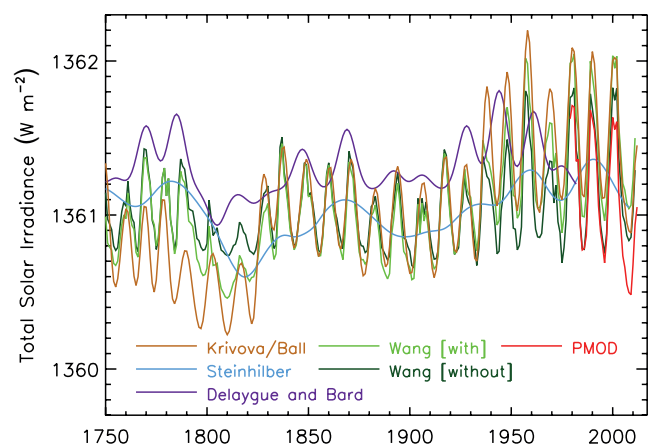


**Figure 8.11** | Reconstructions of total solar irradiance since 1745; annual resolution series from Wang et al. (2005) with and without an independent change in the background level of irradiance, Krivova et al. (2010) combined with Ball et al. (2012) and 5-year time resolution series from Steinhilber et al. (2009) and Delaygue and Bard (2011). The series are standardized to the Physikalisch-Meteorologisches Observatorium Davos (PMOD) measurements of solar cycle 23 (1996–2008) (PMOD is already standardized to Total Irradiance Monitor).

Ball et al., 2012) and sunspot umbra and penumbra and faculae (Ball et al., 2012), or cosmogenic isotopes (Steinhilber et al., 2009; Delaygue and Bard, 2011). These reconstructions are standardized to PMOD SC 23 (1996–2008) (see also Supplementary Material Section 8.SM.6).

For the MM-to-present AR4 gives a TOA instantaneous RF range of 0.1 to 0.28 W m<sup>-2</sup>, equivalent to 0.08 to 0.22 W m<sup>-2</sup> with the RF definition used here. The reconstructions in Schmidt et al. (2011) indicate a MM-to-present RF range of 0.08 to 0.18 W m<sup>-2</sup>, which is within the AR4 range although narrower. As discussed above, the estimates based on irradiance changes in Sun-like stars are not included in this range because the methodology has been shown to be flawed. A more detailed explanation of this is found in Supplementary Material Section 8.SM.6. For details about TSI reconstructions on millennia time scales see Section 5.2.1.2.

#### 8.4.1.3 Attempts to Estimate Future Centennial Trends of Total Solar Irradiance

Cosmogenic isotope and sunspot data (Rigozo et al., 2001; Solanki and Krivova, 2004; Abreu et al., 2008) reveal that currently the Sun is in a grand activity maximum that began about 1920 (20th century grand maximum). However, SC 23 showed an activity decline not previously seen in the satellite era (McComas et al., 2008; Smith and Balogh, 2008; Russell et al., 2010). Most current estimations suggest that the forthcoming solar cycles will have lower TSI than those for the past 30 years (Abreu et al., 2008; Lockwood et al., 2009; Rigozo et al., 2010; Russell et al., 2010). Also there are indications that the mean magnetic field in sunspots may be diminishing on decadal level. A linear expansion of the current trend may indicate that of the order of half the sunspot activity may disappear by about 2015 (Penn and Livingston, 2006). These studies only suggest that the Sun may have left the 20th century grand maximum and not that it is entering another grand minimum. But other works propose a grand minimum during the 21st century, estimating an RF within a range of -0.16 to 0.12 W m<sup>-2</sup> between this future minimum and the present-day TSI (Jones et al., 2012). However, much more evidence is needed and at present there is *very low confidence* concerning future solar forcing estimates.

Nevertheless, even if there is such decrease in the solar activity, there is a *high confidence* that the TSI RF variations will be much smaller in magnitude than the projected increased forcing due to GHG (see Section 12.3.1).

#### 8.4.1.4 Variations in Spectral Irradiance

##### 8.4.1.4.1 Impacts of ultraviolet variations on the stratosphere

Ozone is the main gas involved in stratospheric radiative heating. Ozone production rate variations are largely due to solar UV irradiance changes (HAIGH, 1994), with observations showing statistically significant variations in the upper stratosphere of 2 to 4% along the SC (Soukharev and Hood, 2006). UV variations may also produce transport-induced ozone changes due to indirect effects on circulation (Shindell et al., 2006b). In addition, statistically significant evidence for an 11-year variation in stratospheric temperature and zonal winds is attributed to UV radiation (Frame and Gray, 2010). The direct UV heat-

ing of the background ozone is dominant and over twice as large as the ozone heating in the upper stratosphere and above, while indirect solar and terrestrial radiation through the SC-induced ozone change is dominant below about 5 hPa (Shibata and Kodera, 2005). The RF due to solar-induced ozone changes is a small fraction of the solar RF discussed in Section 8.4.1.1 (Gray et al., 2009).

##### 8.4.1.4.2 Measurements of spectral irradiance

Solar spectral irradiance (SSI) variations in the far (120 to 200 nm) and middle (200 to 300 nm) ultraviolet (UV) are the primary driver for heating, composition, and dynamic changes of the stratosphere, and although these wavelengths compose a small portion of the incoming radiation they show large relative variations between the maximum and minimum of the SC compared to the corresponding TSI changes. As UV heating of the stratosphere over a SC has the potential to influence the troposphere indirectly, through dynamic coupling, and therefore climate (Haigh, 1996; Gray et al., 2010), the UV may have a more significant impact on climate than changes in TSI alone would suggest. Although this indicates that metrics based only on TSI are not appropriate, UV measurements present several controversial issues and modelling is not yet robust.

Multiple space-based measurements made in the past 30 years indicated that UV variations account for about 30% of the SC TSI variations, while about 70% were produced within the visible and infrared (Rottman, 2006). However, current models and data provide the range of 30 to 90% for the contribution of the UV variability below 400 nm to TSI changes (Ermolli et al., 2013), with a more probable value of ~60% (Morrill et al., 2011; Ermolli et al., 2013). The Spectral Irradiance Monitor (SIM) on board SORCE (Harder et al., 2009) shows, over the SC 23 declining phase, measurements that are rather inconsistent with prior understanding, indicating that additional validation and uncertainty estimates are needed (DeLand and Cebula, 2012; Lean and Deland, 2012). A wider exposition can be found in Supplementary Material Section 8.SM.6.

##### 8.4.1.4.3 Reconstructions of preindustrial ultraviolet variations

The Krivova et al. (2010) reconstruction is based on what is known about spectral contrasts of different surface magnetic features and the relationship between TSI and magnetic fields. The authors interpolated backwards to the year 1610 based on sunspot group numbers and magnetic information. The Lean (2000) model is based on historical sunspot number and area and is scaled in the UV using measurements from the Solar Stellar Irradiance Comparison Experiment (SOLSTICE) on board the Upper Atmosphere Research Satellite (UARS). The results show smoothed 11-year UV SSI changes between 1750 and the present of about 25% at about 120 nm, about 8% at 130 to 175 nm, ~4% at 175 to 200 nm, and about 0.5% at 200 to 350 nm. Thus, the UV SSI appears to have generally increased over the past four centuries, with larger trends at shorter wavelengths. As few reconstructions are available, and recent measurements suggest a poor understanding of UV variations and their relationship with solar activity, there is *very low confidence* in these values.

### 8.4.1.5 The Effects of Cosmic Rays on Clouds

Changing cloud amount or properties modify the Earth's albedo and therefore affect climate. It has been hypothesized that cosmic ray flux create atmospheric ions which facilitates aerosol nucleation and new particle formation with a further impact on cloud formation (Dickinson, 1975; Kirkby, 2007). High solar activity means a stronger heliospheric magnetic field and thus a more efficient screen against cosmic rays. Under the hypothesis underlined above, the reduced cosmic ray flux would promote fewer clouds amplifying the warming effect expected from high solar activity. There is evidence from laboratory, field and modelling studies that ionization from cosmic ray flux may enhance aerosol nucleation in the free troposphere (Merikanto et al., 2009; Mirme et al., 2010; Kirkby et al., 2011). However, there is *high confidence (medium evidence and high agreement)* that the cosmic ray-ionization mechanism is too weak to influence global concentrations of cloud condensation nuclei or their change over the last century or during a SC in a climatically significant way (Harrison and Ambaum, 2010; Erlykin and Wolfendale, 2011; Snow-Kropla et al., 2011). A detailed exposition is found in Section 7.4.6.

## 8.4.2 Volcanic Radiative Forcing

### 8.4.2.1 Introduction

Volcanic eruptions that inject substantial amounts of SO<sub>2</sub> gas into the stratosphere are the dominant natural cause of externally forced climate change on the annual and multi-decadal time scales, both because of the multi-decadal variability of eruptions and the time scale of the climate system response, and can explain much of the pre-industrial climate change of the last millennium (Schneider et al., 2009; Brovkin et al., 2010; Legras et al., 2010; Miller et al., 2012). Although volcanic eruptions inject both mineral particles (called ash or tephra) and sulphate aerosol precursor gases (predominantly SO<sub>2</sub>) into the atmosphere, it is the sulphate aerosols, which because of their small size are effective scatterers of sunlight and have long lifetimes, that are responsible for RF important for climate. Global annually averaged emissions of CO<sub>2</sub> from volcanic eruptions since 1750 have been at least 100 times smaller than anthropogenic emissions and inconsequential for climate on millennial and shorter time scales (Gerlach, 2011). To be important for climate change, sulphur must be injected into the stratosphere, as the lifetime of aerosols in the troposphere is only about one week, whereas sulphate aerosols in the stratosphere from tropical eruptions have a lifetime of about one year, and those from high-latitude eruptions last several months. Most stratospheric aerosols are from explosive eruptions that directly put sulphur into the stratosphere, but Bourassa et al. (2012, 2013) showed that sulphur injected into the upper troposphere can then be lifted into the stratosphere over the next month or two by deep convection and large scale Asian summer monsoon circulation, although Vernier et al. (2013) and Fromm et al. (2013) suggested that direct injection was also important. Robock (2000), AR4 (Forster et al., 2007) and Timmreck (2012) provide summaries of this relatively well understood forcing agent.

There have been no major volcanic eruptions since Mt Pinatubo in 1991 (Figure 8.12), but several smaller eruptions have caused a RF for the years 2008–2011 of  $-0.11$  ( $-0.15$  to  $-0.08$ ) W m<sup>-2</sup>, approximately

twice the magnitude of the 1999–2002 RF of  $-0.06$  ( $-0.08$  to  $-0.04$ ) W m<sup>-2</sup>, consistent with the trends noted in Solomon et al. (2011). However, the CMIP5 simulations discussed elsewhere in this report did not include the recent small volcanic forcing in their calculations. New work has also produced a better understanding of high latitude eruptions, the hydrological response to volcanic eruptions (Trenberth and Dai, 2007; Anchukaitis et al., 2010), better long-term records of past volcanism and better understanding of the effects of very large eruptions.

There are several ways to measure both the SO<sub>2</sub> precursor and sulphate aerosols in the stratosphere, using balloons, airplanes, and both ground- and satellite-based remote sensing. Both the infrared and ultraviolet signals sensed by satellite instruments can measure SO<sub>2</sub>, and stratospheric aerosol measurements by space-based sensors have been made on a continuous basis since 1978 by a number of instruments employing solar and stellar occultation, limb scattering, limb emission, and lidar strategies (Thomason and Peter, 2006; Kravitz et al., 2011; Solomon et al., 2011).

Forster et al. (2007) described four mechanisms by which volcanic forcing influences climate: RF due to aerosol–radiation interaction; differential (vertical or horizontal) heating, producing gradients and changes in circulation; interactions with other modes of circulation, such as El Niño–Southern Oscillation (ENSO); and ozone depletion with its effects on stratospheric heating, which depends on anthropogenic chlorine (stratospheric ozone would increase with a volcanic eruption under low-chlorine conditions). In addition, the enhanced diffuse light from volcanic aerosol clouds impacts vegetation and hence the carbon cycle (Mercado et al., 2009) and aerosol–cloud interaction of sulphate aerosols on clouds in the troposphere can also be important (Schmidt et al., 2010), though Frolicher et al. (2011) showed that the impacts of the 1991 Mt Pinatubo eruption on the carbon cycle were small.

### 8.4.2.2 Recent Eruptions

The background stratospheric aerosol concentration was affected by several small eruptions in the first decade of the 21st century (Nagai et al., 2010; Vernier et al., 2011; Neely et al., 2013; see also Figure 8.13), with a very small contribution from tropospheric pollution (Siddaway and Petelina, 2011; Vernier et al., 2011), and had a small impact on RF (Solomon et al., 2011). Two recent high-latitude eruptions, of Kasatochi Volcano (52.1°N, 175.3°W) on August 8, 2008 and of Sarychev Volcano (48.1°N, 153.2°E) on June 12–16, 2009, each injected ~1.5 Tg(SO<sub>2</sub>) into the stratosphere, but did not produce detectable climate response. Their eruptions, however, led to better understanding of the dependence of the amount of material and time of year of high-latitude injections to produce climate impacts (Haywood et al., 2010; Kravitz et al., 2010, 2011). The RF from high-latitude eruptions is a function of seasonal distribution of insolation and the 3- to 4-month lifetime of high-latitude volcanic aerosols. Kravitz and Robock (2011) showed that high-latitude eruptions must inject at least 5 Tg(SO<sub>2</sub>) into the lower stratosphere in the spring or summer, and much more in fall or winter, to have a detectable climatic response.

On April 14, 2010 the Eyjafjallajökull volcano in Iceland (63.6°N, 19.6°W) began an explosive eruption phase that shut down air traffic



in Europe for 6 days and continued to disrupt it for another month. The climatic impact of Eyjafjallajökull was about 10,000 times less than that of Mt Pinatubo; however, because it emitted less than 50 ktonnes  $\text{SO}_2$  and its lifetime in the troposphere was 50 times less than if it had been injected into the stratosphere, and was therefore undetectable amidst the chaotic weather noise in the atmosphere (Robock, 2010). 2011 saw the continuation of a number of small eruptions with significant tropospheric  $\text{SO}_2$  and ash injections, including Puyehue-Cordón Caulle in Chile, Nabro in Eritrea, and Grimsvötn in Iceland. None have been shown to have produced an important RF, but the June 13, 2011 Nabro eruption resulted in the largest stratospheric aerosol cloud since the 1991 Mt Pinatubo eruption (Bourassa et al., 2012), more than 1.5  $\text{Tg}(\text{SO}_2)$ .

Figure 8.12 shows reconstructions of volcanic aerosol optical depth since 1750. Figure 8.13 shows details of the vertical distribution of stratospheric aerosols in the tropics since 1985. The numerous small eruptions in the past decade are evident, but some of them were at higher latitudes and their full extent is not captured in this plot.

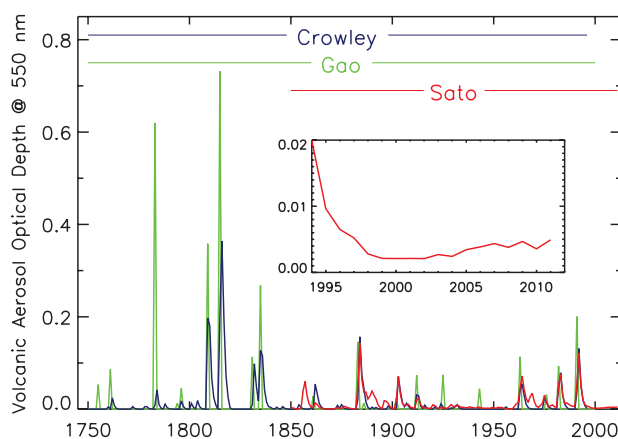


**Figure 8.12** | Volcanic reconstructions of global mean aerosol optical depth (at 550 nm). Gao et al. (2008) and Crowley and Unterman (2013) are from ice core data, and end in 2000 for Gao et al. (2008) and 1996 for Crowley and Unterman (2013). Sato et al. (1993) includes data from surface and satellite observations, and has been updated through 2011. (Updated from Schmidt et al., 2011.)

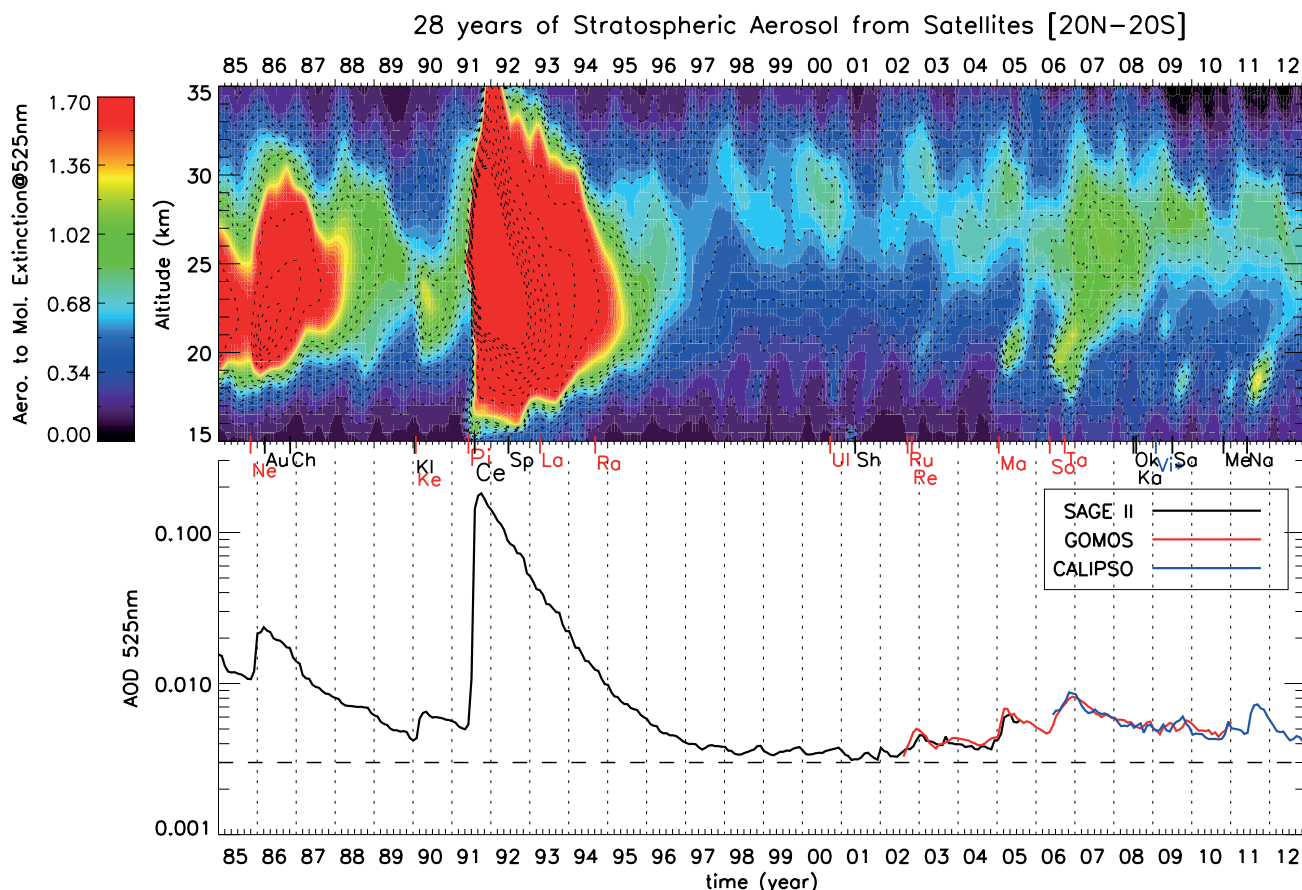


**Figure 8.13** | (Top) Monthly mean extinction ratio (525 nm) profile evolution in the tropics [20°N to 20°S] from January 1985 through December 2012 derived from Stratospheric Aerosol and Gas Experiment (SAGE) II extinction in 1985–2005 and Cloud-Aerosol Lidar and Infrared Pathfinder Satellite Observation (CALIPSO) scattering ratio in 2006–2012, after removing clouds below 18 km based on their wavelength dependence (SAGE II) and depolarization properties (CALIPSO) compared to aerosols. Black contours represent the extinction ratio in log-scale from 0.1 to 100. The position of each volcanic eruption occurring during the period is displayed with its first two letters on the horizontal axis, where tropical eruptions are noted in red. The eruptions were Nevado del Ruiz (Ne), Augustine (Au), Chikurachki (Ch), Kliuchevskoi (Ki), Kelut (Ke), Pinatubo (Pi), Cerro Hudson (Ce), Spur (Sp), Lascar (La), Rabaul (Ra), Ulawun (UI), Shiveluch (Sh), Ruang (Ru), Reventador (Re), Manam (Ma), Soufrière Hills (So), Tavorvur (Ta), Okmok (Ok), Kasatochi (Ka), Victoria (Vi)—forest fires with stratospheric aerosol injection), Sarychev (Sa), Merapi (Me), Nabro (Na). (Updated from Figure 1 from Vernier et al., 2011.) (Bottom) Mean stratospheric aerosol optical depth (AOD) in the tropics [20°N to 20°S] between the tropopause and 40 km since 1985 from the SAGE II (black line), the Global Ozone Monitoring by Occultation of Stars (GOMOS) (red line), and CALIPSO (blue line). (Updated from Figure 5 from Vernier et al., 2011.)

### Box 8.3 | Volcanic Eruptions as Analogues

Volcanic eruptions provide a natural experiment of a stratospheric aerosol cloud that can serve to inform us of the impacts of the proposed production of such a cloud as a means to control the climate, which is one method of geoengineering (Rasch et al., 2008); see Section 7.7. For example, Trenberth and Dai (2007) showed that the Asian and African summer monsoon, as well as the global hydrological cycle, was weaker for the year following the 1991 Mt Pinatubo eruption, which is consistent with climate model simulations (Robock et al., 2008). MacMynowski et al. (2011) showed that because the climate system response of the hydrological cycle is rapid, forcing from volcanic eruptions, which typically last about a year, can serve as good analogues for longer-lived forcing. The formation of sulphate aerosols, their transport and removal, their impacts on ozone chemistry, their RF, and the impacts on whitening skies all also serve as good analogues for geoengineering proposals. Volcanic impacts on the carbon cycle because of more diffuse radiation (Mercado et al., 2009) and on remote sensing can also be useful analogues, and the impacts of contrail-generated sub-visual cirrus (Long et al., 2009) can be used to test the long-term impacts of a permanent stratospheric cloud.

Smoke from fires generated by nuclear explosions on cities and industrial areas, which could be lofted into the stratosphere, would cause surface cooling and a reduction of stratospheric ozone (Mills et al., 2008). Volcanic eruptions that produce substantial stratospheric aerosol clouds also serve as an analogue that supports climate model simulations of the transport and removal of stratospheric aerosols, their impacts on ozone chemistry, their RF, and the climate response. The use of the current global nuclear arsenal still has the potential to produce nuclear winter, with continental temperatures below freezing in summer (Robock et al., 2007a; Toon et al., 2008), and the use of only 100 nuclear weapons could produce climate change unprecedented in recorded human history (Robock et al., 2007b), with significant impacts on global agriculture (Özdoğan et al., 2013; Xia and Robock, 2013).

#### 8.4.2.3 Records of Past Volcanism and Effects of Very Large Eruptions

Although the effects of volcanic eruptions on climate are largest in the 2 years following a large stratospheric injection, and the winter warming effect in the NH has been supported by long-term records (Fischer et al., 2007), there is new work indicating extended volcanic impacts via long-term memory in the ocean heat content and sea level (Stenchikov et al., 2009; Gregory, 2010; Otterä et al., 2010). Zanchettin et al. (2012) found changes in the North Atlantic Ocean circulation that imply strengthened northward oceanic heat transport a decade after major eruptions, which contributes to the emergence of extensive winter warming over the continental NH along with persistent cooling over Arctic regions on decadal time scales, in agreement with Zhong et al. (2011) and Miller et al. (2012).

New work on the mechanisms by which a supereruption (Self and Blake, 2008) could force climate has focused on the 74,000 BP eruption of the Toba volcano (2.5°N, 99.0°E). Robock et al. (2009) used simulations of up to 900 times the 1991 Mt Pinatubo sulphate injection to show that the forcing is weaker than that predicted based on a linear relationship with the sulphate aerosol injection. The results agreed with a previous simulation by Jones et al. (2005). They also showed that chemical interactions with ozone had small impacts on the forcing and that the idea of Bekki et al. (1996) that water vapour would limit and prolong the growth of aerosols was not supported. Timmreck et al. (2010) however, incorporating the idea of Pinto et al. (1989) that aerosols would grow and therefore both have less RF per unit mass and fall out of the atmosphere more quickly, found much less of a radiative impact from such a large stratospheric input.

#### 8.4.2.4 Future Effects

We expect large eruptions over the next century but cannot predict when. Ammann and Naveau (2003) and Stothers (2007) suggested an 80-year periodicity in past eruptions, but the data record is quite short and imperfect, and there is no mechanism proposed that would cause this. While the period 1912–1963 was unusual for the past 500 years in having no large volcanic eruptions, and the period 1250–1300 had the most globally climatically significant eruptions in the past 1500 years (Gao et al., 2008), current knowledge only allows us to predict such periods on a statistical basis, assuming that the recent past distributions are stationary. Ammann and Naveau (2003), Gusev (2008), and Deligne et al. (2010) studied these statistical properties and Ammann and Naveau (2010) showed how they could be used to produce a statistical distribution for future simulations. Although the future forcing from volcanic eruptions will depend only on the stratospheric aerosol loading for most forcing mechanisms, the future effects on reducing ozone will diminish as ozone depleting substances diminish in the future (Eyring et al., 2010b).

## 8.5 ~~Synthesis of Global Mean Radiative Forcing, Past and Future~~

~~The RF can be used to quantify the various agents that drive climate change over the Industrial Era or the various contributions to future climate change. There are multiple ways in which RF can be attributed to underlying causes, each providing various perspectives on the importance of the different factors driving climate change. This section evaluates the RF with respect to emitted component and with respect to the ultimate atmospheric concentrations. The uncertainties in the RF~~